Numerical modelling of one- and two-dimensional bandgap structures

Toni Okuogume

School of Electrical Engineering

Thesis submitted for examination for the degree of Master of Science in Technology.

Espoo 10.10.2016

Thesis supervisor:

Prof. Ari Sihvola

Thesis advisor:

PhD Pasi Ylä-Oijala

Aalto University
School of Electrical
Engineering

AALTO UNIVERSITY
SCHOOL OF ELECTRICAL ENGINEERING

ABSTRACT OF THE
MASTER'S THESIS

Author: Toni Okuogume

Title: Numerical modelling of one- and two-dimensional bandgap structures

Date: 10.10.2016 Language: English Number of pages: 7+32

Department of Radio Science and Technology

Professorship: Electromagnetics

Supervisor: Prof. Ari Sihvola

Advisor: PhD Pasi Ylä-Oijala

Bandgap structures are materials made by combining simple elements to form a periodic lattice. When the dielectric contrast between the elements and the background is large enough, the structure will filter certain wavelengths thus forming stopbands for electromagnetic waves. This kind of property is used for example in mirrors, filters and in thermal insulation applications.
In this thesis, methods of theoretically analysing one- and two-dimensional bandgap structures are shown. One-dimensional structures can be solved with pure analytical calculations, but analysing two-dimensional form requires numerical approach. The numerical approach that was chosen was Finite Element Method. Besides the ideal case of an infinite structure, structures with finite amount of elements and structures with defect elements where studied.

Keywords: Bandgap structures, Electromagnetics, Filters, Finite Element Method, Numerical modeling, Periodic structures, Photonic crystals

AALTO-YLIOPISTO
SÄHKÖTEKNIIKAN KORKEAKOULU

DIPLOMITYÖN
TIIVISTELMÄ

Tekijä: Toni Okuogume

Työn nimi: Yksi- ja kaksiulotteisten estokaistarakenteiden numeerinen mallinnus

Päivämäärä: 10.10.2016 Kieli: Englanti Sivumäärä: 7+32

Radiotieteen ja -tekniikan laitos

Professuuri: Sähkömagnetiikka

Työn valvoja: Prof. Ari Sihvola

Työn ohjaaja: FT Pasi Ylä-Oijala

Estokaistarakenteet ovat materiaaleja jotka on muodostettu yhdistelemällä yksinkertaisia elementtejä säännölliseen hilaan. Kun elementtien ja tausta-aineen välinen dielektrinen kontrasti on riittävän suuri, rakenne heijastaa tiettyjä taajuusalueita täten muodostaen estokaistoja. Tämä ominaisuus on hyvin hyödyllinen mm. peileissä, suodattimissa ja lämpöeristerakenteissa.
Tässä diplomityössä tutkitaan teoreettisesti yksi- ja kaksiulotteisia estokaistarakenteita. Yksiulotteisia rakenteita voi tarkastella puhtaasti analyyttisten kaavojen avulla, mutta kaksiulotteisten rakenteiden analysointi vaatii numeerista käsittelyä, mihin tässä työssä käytettiin elementtimenetelmää. Ideaalisen äärettömän useasta elementistä koostuvan rakenteen lisäksi työssä tutkittiin rakenteita, joissa on äärellinen määrä elementtejä sekä rakenteita joiden hilassa on kidevirheitä.

Avainsanat: Elementtimenetelmä, Estokaistarakenteet, Fotonikiderakenteet, Numeerinen mallinnus, Periodiset rakenteet, Suodattimet, Sähkömagnetiikka

Preface

This thesis work has been done for Electromagnetics research group of the Department of Radio Science and Technology at Aalto University School of Electrical Engineering. Work was financed by Aalto Energy Efficiency Programme EXPECTS project.

I want to thank Professor Ari Sihvola and my instructor PhD Pasi Ylä-Oijala for all teaching, guidance and especially patience for the long journey this work has been. I also want to thank EXPECTS project for providing me interesting topic to study.

Lastly I want to thank my sisters and my father for all the support they have given to me and especially my mother who has always believed in me even when I have not.

Tapiola, October 10, 2016

Toni Okuogume

Contents

Symbols and abbreviations

Symbols

$\mathbf{E}$	electric field
$\mathbf{B}$	magnetic displacement
$\mathbf{H}$	magnetic field
$\mathbf{D}$	electric displacement
$\mathbf{J}$	electric current density
ρ	electric charge density
ϵ	dielectric permittivity
μ	magnetic permeability
c	speed of light 299 792 458 [m/s]

Operators

$\nabla \times \mathbf{A}$	curl of vector $\mathbf{A}$
$\frac{\partial}{\partial t}$	partial derivative with respect to variable t
$\nabla \cdot \mathbf{A}$	divergence of vector $\mathbf{A}$
$\sum_i$	sum over index i
$\mathbf{A} \cdot \mathbf{B}$	dot product of vectors $\mathbf{A}$ and $\mathbf{B}$
$\mathbf{A} \times \mathbf{B}$	vector product of vectors $\mathbf{A}$ and $\mathbf{B}$

Abbreviations

TE	transverse electric
TM	transverse magnetic
FDTD	Finite-Difference Time-Domain Method
FEM	Finite Element Method
TMM	Transfer Matrix Method

1 Introduction

Bandgap structures were first introduced by Yablonovitch [1]. They are structures with infinitely repeating patters. For example in one-dimensional case this means a repeating layer structure. This periodicity makes the bandgap structure impermeable to electromagnetic waves of certain wavelength. The prohibited wavelength band i.e. the stopband of the structure depends on the materials of the bandgap structure and the size of the periodic unit cell of the structure.

There are a lot of different potential applications for bandgap structures depending on different frequency ranges. In the optical spectrum there is vast interest in optical circuits that could potentially replace some of the electric circuits in the future. In the infrared region there is a lot of interest using bandgap structures to enhance the efficiency of solar panels.[2] Bandgap structures can be even found in nature. For example [3] male peacock feathers shine in bright colours because of the nanostructures in them. Periodic nanostructures can be found also in some tropical fish scales, in beetles, in butterfly wings etc.

Figure 1: Male peacock feathers are one of the places in nature where there are periodic nanostructures [3]

In this work the electromagnetic wave reflection properties of the bandgap structures are studied. Structures are studied in both one-dimensional and in two-dimensional cases. In one-dimensional case where the structures are multilayer structures accurate analytical solutions can be derived. With two-dimensional case number and shape of the possible geometries makes numerical approach necessary in all but the most simple cases.

2 Electromagnetic waves in periodic media

2.1 Introduction

Inspection of the behaviour of electromagnetic waves in periodic media starts with Maxwell's equations. These fundamental equations are perfectly analytical expressions of electromagnetic waves behaviour in arbitrary media. The equations are

$$\nabla \times \mathbf{E}(\mathbf{r}, t) = -\frac{\partial}{\partial t}\mathbf{B}(\mathbf{r}, t) \tag{1}$$

$$\nabla \times \mathbf{H}(\mathbf{r}, t) = \frac{\partial}{\partial t}\mathbf{D}(\mathbf{r}, t) + \mathbf{J}(\mathbf{r}, t) \tag{2}$$

$$\nabla \cdot \mathbf{D}(\mathbf{r}, t) = \rho(\mathbf{r}, t) \tag{3}$$

$$\nabla \cdot \mathbf{B}(\mathbf{r}, t) = 0 \tag{4}$$

where $\mathbf{E}$ is the electric field, $\mathbf{B}$ is the magnetic flux density, $\mathbf{H}$ is the magnetic field, $\mathbf{J}$ is the current density and $\mathbf{D}$ is the electric displacement field. [4] Magnetic flux density and electric displacement field are connected to electric and magnetic field via constitutive relations that are in linear and isotropic material

$$\mathbf{D} = \epsilon\mathbf{E} \tag{5}$$

$$\mathbf{B} = \mu\mathbf{H}, \tag{6}$$

where $\epsilon = \epsilon_r\epsilon_0$ is the dielectric permittivity and $\mu = \mu_r\mu_0$ is the magnetic permeability. $\epsilon_0 = 8.8541878176 \times 10^{-12} F/m$ is the permittivity of free space and $\mu_0 = 4\pi \times 10^{-7} H \cdot m^{-1}$ is the permeability of free space and ϵ_r and μ_r are the relative permittivity and permeability. Consider that we are dealing with time-harmonic waves. In that case the fields are in the form of

$$\mathbf{A}(\mathbf{r}, t) = \mathbf{A}(\mathbf{r})e^{j\omega t} \tag{7}$$

which means that the time derivative gives $\frac{\partial}{\partial t} = j\omega$ for all fields. Because every field quantity has the same time dependency we can subtract it from the equations. It is also assumed that all materials are isotropic and piece-wise homogeneous and there is no free charges or current in the region of interest. Thus, we can remove $\mathbf{J}$ from equation (2) and ρ from equation (3).

By combining these with Maxwell's equations forms the source-free Maxwell's equations for time-harmonic fields

$$\nabla \times \mathbf{E} = -j\omega\mu\mathbf{H} \tag{8}$$

$$\nabla \times \mathbf{H} = j\omega\epsilon\mathbf{E} \tag{9}$$

$$\nabla \cdot \mathbf{D} = 0 \tag{10}$$

$$\nabla \cdot \mathbf{B} = 0 \tag{11}$$

These equations hold true in the interior of a homogeneous material. On an interface between two materials with different dielectric properties the fields should satisfy the interface conditions which leads to that the tangential components of the electric and magnetic fields has to be continuous

$$\mathbf{n} \times (\mathbf{E}_1 - \mathbf{E}_2) = 0 \tag{12}$$

$$\mathbf{n} \times (\mathbf{H}_1 - \mathbf{H}_2) = 0 \tag{13}$$

One important issue is the polarization of a wave. In the context of this work this means how the electric and magnetic fields are directed against the structure as they travel through the medium. Without losing generality, we can focus on linear polarization where we can treat separately two linear polarizations. Solutions for a general polarization can be obtained as a linear combination of these cases. The two cases are the transverse electric (TE) and the transverse magnetic (TM). In this work TE mode means that the electric field is perpendicular to the plane of incidence which is the interface between two dielectric material and TM vice versa.

When a wave is travelling through a dielectric medium, which is usually modelled as air, and confronts another dielectric material, part of the wave is reflected back and part goes through the interface. Dielectric materials can be characterised with characteristic impedance

$$\eta_i = \sqrt{\frac{\mu_i}{\epsilon_i}}, \tag{14}$$

where i is the layer number. Assume that an electromagnetic wave travels through the space and encounters an infinitive slab of dielectric material without any losses. Refraction occurring on the interface of the two different dielectric materials can be analysed by using Snell's law

$$n_1 \sin\theta_1 = n_2 \sin\theta_2 \tag{15}$$

The reflection coefficient R is the ratio of the reflected wave amplitude to the incident wave amplitude

$$R = \frac{E_{1-}}{E_{1+}} = \frac{\eta_2 - \eta_1}{\eta_2 + \eta_1} \tag{16}$$

and the transmission coefficient T is the ratio of the transmitted wave amplitude to incident wave amplitude

$$T = 1 - R = \frac{E_{2+}}{E_{1+}} = \frac{2\eta_2}{\eta_2 + \eta_1} \tag{17}$$

2.2 Solid-state physics notation

Electromagnetic bandgap structures share many similarities with crystal structures in solid-state physics. Crystal structures in solid-state physics are infinite periodic atom structures where the electron wave travels and reacts with periodic potentials of atoms.[5] Because of these similarities we can borrow the notations and methods used in solid-state physics to analyse electromagnetic bandgap structures.

The concept of stopbands and passbands is central. Stopbands are the frequency ranges where there are no travelling waves in the structure. Passbands are the frequencies where the electromagnetic wave can enter and travel in the structure.

Figure 2 shows a two-dimensional bandgap structure with infinitive long dielectric cylinders in air. The smallest possible structure that can be infinitely copied to form the whole structure is called a *unit cell*. The space where all unit cells lies can be called lattice space. Vector $\mathbf{R} = l\mathbf{a}_1 + m\mathbf{a}_2 + n\mathbf{a}_3$ that points from one unit cell point to similar point in another unit cell is called a lattice vector where vectors $\mathbf{a}_1, \mathbf{a}_2, \mathbf{a}_3$ are the basis vectors of the lattice.

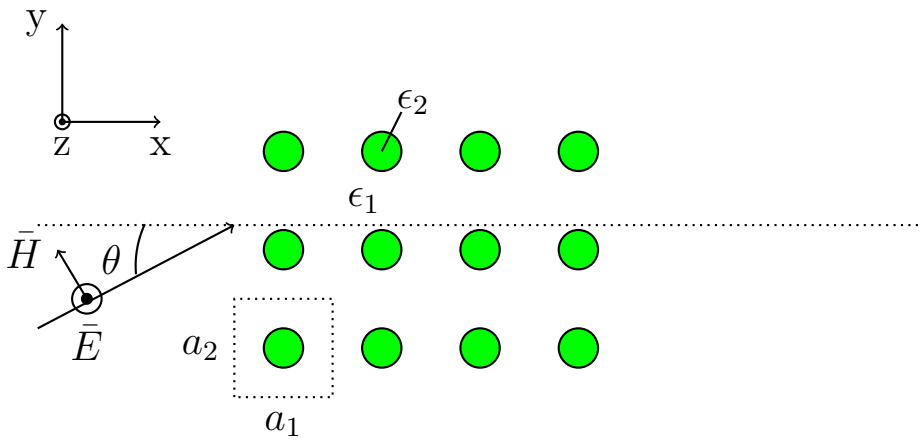

Figure 2: Two-dimensional bandgap structure

A bandgap structure [6] has periodic permittivity

$$\epsilon(\mathbf{r}) = \sum_{\mathbf{G}} \epsilon(\mathbf{G}) e^{j\mathbf{G}\cdot\mathbf{r}} \tag{18}$$

Because of the periodicity constraint, the permittivity function must fulfil the following condition

$$\epsilon(\mathbf{r}+\mathbf{R}) = \sum_{\mathbf{G}} \epsilon(\mathbf{G}) e^{j\mathbf{G}\cdot\mathbf{r}} e^{j\mathbf{G}\cdot\mathbf{R}} = \epsilon(\mathbf{r}) \tag{19}$$

To study the dispersion relation of a bandgap structure we need to use the concept of a reciprocal lattice. Assume that there are arbitrary reciprocal lattice vectors $\mathbf{G}$ which are of the form $\mathbf{G} = l\mathbf{b}_1 + m\mathbf{b}_2 + n\mathbf{b}_3$ and conform to the following requirement with primitive lattice vectors

$$\mathbf{G}\cdot\mathbf{R} = 2\pi N \tag{20}$$

Because of the constraint, the basis vectors of the reciprocal lattice vector's are

$$\mathbf{b_1} = \frac{2\pi\mathbf{a}_2\times\mathbf{a}_3}{\mathbf{a}_1\cdot(\mathbf{a}_2\times\mathbf{a}_3)}, \quad \mathbf{b_2} = \frac{2\pi\mathbf{a}_3\times\mathbf{a}_1}{\mathbf{a}_1\cdot(\mathbf{a}_2\times\mathbf{a}_3)}, \quad \mathbf{b_3} = \frac{2\pi\mathbf{a}_1\times\mathbf{a}_2}{\mathbf{a}_1\cdot(\mathbf{a}_2\times\mathbf{a}_3)} \tag{21}$$

These basis vectors form the basis of a reciprocal lattice. Calculating a reciprocal lattice of a given reciprocal lattice gives the original lattice. A reciprocal lattice can have different geometry depending on the original lattice. For example reciprocal lattice of triangle lattice is a triangle lattice that is rotated compared to the original lattice.

In a similar way as the permittivity in the bandgap structure, the electric field mode can be expressed as

$$\tilde{\mathbf{E}} = \mathbf{E}_\mathbf{k}(\mathbf{r}) e^{-j\mathbf{k}\cdot\mathbf{r}} \tag{22}$$

where the complex amplitude function is periodic

$$\mathbf{E}_\mathbf{k}(\mathbf{r}) = \mathbf{E}_\mathbf{k}(\mathbf{r}+\mathbf{R}) \tag{23}$$

These can be combined to get Floquet-Bloch Theorem stating that the electric field in a periodic medium fulfills the condition

$$\tilde{\mathbf{E}}(\mathbf{r}+\mathbf{R}) = e^{i\mathbf{k}\cdot\mathbf{R}}\tilde{\mathbf{E}}(\mathbf{r}) \tag{24}$$

If we add a reciprocal lattice vector $\mathbf{G}$ to $\mathbf{k}$, the electric field mode stays the same. This means that all unique solutions to the electric mode in bandgap structures are inside a zone where we can't get by adding a reciprocal lattice vector to the Bloch wave vector. This zone is called the (first) Brillouin zone. Visually this is the zone that is got by picking a lattice point of the origin in the reciprocal lattice and a drawing line in the middle of it and all the neighboring lattice points as illustrated in Figure 3.

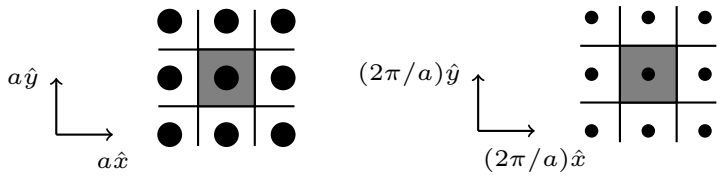

Figure 3: The first Brillouin zone for square lattice (left) and it's reciprocal lattice (right)

2.3 One-dimensional bandgap structures

2.3.1 Introduction

One-dimensional bandgap structures, or multilayer film structures, are structures where we have two different materials layered on top each other. One of the earlier applications of multilayer films are so called Bragg mirrors or quarter-wave stacks. These structure are multilayer films where each film has the width of a quarter of the wavelength of the central frequency of an incoming wave. These structures are used for example in anti-reflective coatings.

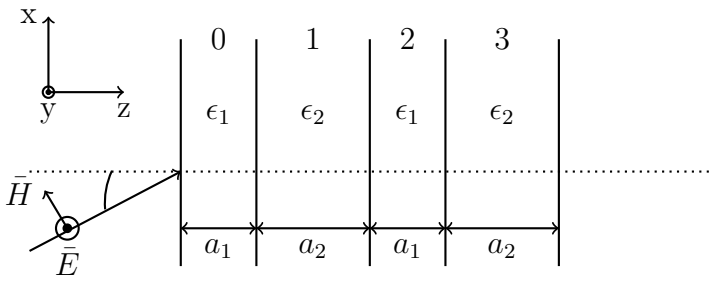

Figure 4: Finite multilayer film

Examination of multilayer films can be separated to two cases: The on-axis case where the incoming wave is parallel to the surface normal of the boundary, and the off-axis case where there is an angle between the incoming wave and the surface normal. A structure is illustrated in Figure 4. Every layer is assumed to be infinite in the xy-plane. The number of layers can be finite or infinite depending on the simulation.

2.3.2 On-axis propagation

Assume that we have an infinitive stack of alternating dielectric layers as shown in Figure 4. The dielectric constants of the layers are ϵ_1 and ϵ_2 and the widths are a_1 and a_2 with combined width for one periodic pair d. The layers are assumed to be nonmagnetic so $\mu_r = 1$ in every layer. A time-harmonic electromagnetic wave is travelling to z-direction

$$\mathbf{E}(z) = \mathbf{E}e^{-jk_z z} \qquad \mathbf{H}(z) = \mathbf{H}e^{-jk_z z} \tag{25}$$

When an electromagnetic wave hits a boundary between two materials with different dielectric properties, part of the wave is reflected back and part of it goes through. This means that inside every layer there is forwards, and backwards, propagating wave components

$$\mathbf{E}(\mathbf{r}) = \mathbf{E}_+(\mathbf{r}) + \mathbf{E}_-(\mathbf{r}) \tag{26}$$

$$\mathbf{E}(\mathbf{r}) = E(z)\mathbf{u}_x \tag{27}$$

From equation (12) we know that the tangential components on the both sides of the boundary have to be same. The tangential components of the total electric field on the both sides of an interface can be expressed as

$$E_1 = a_1 e^{jk_{z1}z} + b_1 e^{-jk_{z2}z} \tag{28}$$

$$E_2 = a_2 e^{jk_{z1}z} + b_2 e^{-jk_{z2}z} \tag{29}$$

where E_1 and E_2 are the field amplitudes in layer 1 and 2 respectively. As the waves move only in z-axis we can simplify the differential operator to

$$\nabla = \frac{\partial}{\partial z}\mathbf{u}_z \tag{30}$$

To compose equations for the magnetic field, simplified nabla (30) is used with equation (8) and (28)

$$\mathbf{H} = \frac{\nabla \times \mathbf{E}}{-j\omega\mu} \tag{31}$$

$$H_1 = -\frac{k_{z1}}{\omega\mu} a_1 e^{jk_{z1}z} + \frac{k_{z1}}{\omega\mu} b_1 e^{-jk_{z1}z} \tag{32}$$

Equations (12) and (13) force the tangential components of the electric and magnetic fields to be equal on both sides of the interface, i.e,

$$E_1(z_n) = E_2(z_n) \qquad H_1(z_n) = H_2(z_n) \tag{33}$$

Using time harmonic Maxwell's equations with notations from equation (28), interface constrains become

$$a_1 + b_1 = a_2 e^{-ik_{z2}a_2} + b_2 e^{-ik_{z2}a_2} \tag{34}$$

$$a_1 - b_1 = \frac{k_{z2}}{k_{z1}} \left[a_2 e^{-ik_{z2}a_2} - b_2 e^{-ik_{z2}a_2} \right] \tag{35}$$

Since we have four unknowns(a_1, b_1, a_2, b_2) but only two equations, to get more equations we use the interface constrains of the previous boundary of the bandgap structure

$$a_0 + b_0 = a_1 e^{-ik_{z1}a_1} + b_1 e^{-ik_{z1}a_1} \tag{36}$$

$$a_0 - b_0 = \frac{k_{z1}}{k_{z2}} \left[a_1 e^{-ik_{z1}a_1} - b_1 e^{-ik_{z1}a_1} \right] \tag{37}$$

To reduce the number of unknowns to be same as the number of equations, the Floquet-Bloch (24) theorem is used with the equations, i.e,

$$E(z + d) = e^{ik_b d} E(z) \qquad H(z + d) = e^{ik_b d} H(z), \tag{38}$$

where k_b is the Floquet-Bloch wave vector. After using (38), the final result is a four equation system with four unknowns. The solution to this system is the characteristic equation that is formed by calculating the zero point for the determinant of the matrix equation. The characteristic equation will reduce to

$$\cos(k_b(a_1 + a_2)) = \cos k_{z1}a_1 \cos k_{z2}a_2 - \frac{k_{z1}^2 + k_{z2}^2}{2k_{z1}k_{z2}} \sin k_{z1}a_1 \sin k_{z2}a_2 \tag{39}$$

The left side of the equation is always between 1 and -1. The frequencies that don't fulfil this equation are the bandgaps for the one-dimensional structure. [7]

In on-axis propagation there is no difference between TE and TM polarisations of the electromagnetic wave.

2.3.3 Off-axis propagation

The more complicated case is when the wave vector of the incoming electromagnetic wave is not parallel to the normal of the boundary. Now the waves are of the form

$$\mathbf{E}(\mathbf{r}) = \mathbf{E} e^{-j\mathbf{k}\cdot\mathbf{r}} \qquad \mathbf{H}(\mathbf{r}) = \mathbf{H} e^{-j\mathbf{k}\cdot\mathbf{r}} \tag{40}$$

When the wave encounters a dielectric interface obliquely, equations for the reflected and transmitted wave need to be modified. There are two cases, shown in Figure 5,

that depend on the electric and magnetic field directions: transverse electric (TE) where the electric field is perpendicular to the plane of incidence and transverse magnetic (TM) where the magnetic field is perpendicular to the interface.

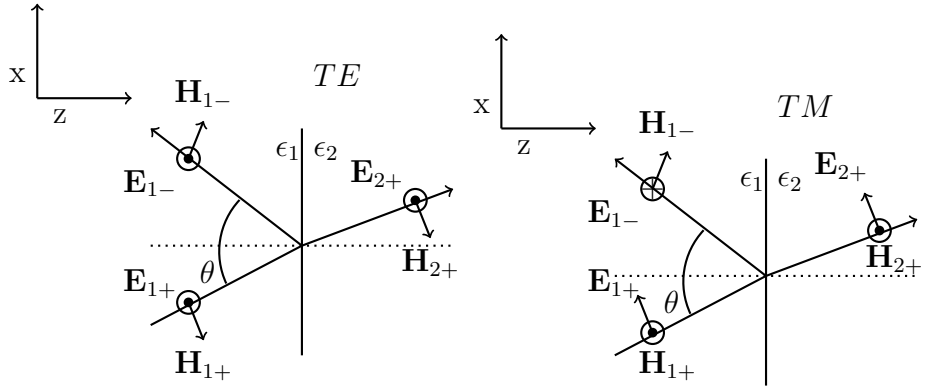

Figure 5: Illustration of the electromagnetic waves in the TE(left) and TM(right) modes when reflected from a boundary

For TE mode the incident waves are

$$\mathbf{E}_{1+}(\mathbf{r}) = \mathbf{u}_y E_{1+} e^{-j\mathbf{k}_{1+}\cdot\mathbf{r}} \tag{41}$$

$$\mathbf{H}_{1+}(\mathbf{r}) = (\mathbf{u}_z \sin\theta_1 - \mathbf{u}_x \cos\theta_1)\frac{E_{1+}}{\eta_1} e^{-j\mathbf{k}_{1+}\cdot\mathbf{r}} \tag{42}$$

and the reflected waves are

$$\mathbf{E}_{1-}(\mathbf{r}) = \mathbf{u}_y E_{1-} e^{-j\mathbf{k}_{1+}\cdot\mathbf{r}} \tag{43}$$

$$\mathbf{H}_{1-}(\mathbf{r}) = (\mathbf{u}_z \sin\theta_1 + \mathbf{u}_x \cos\theta_1)\frac{E_{1-}}{\eta_1} e^{-j\mathbf{k}_{1-}\cdot\mathbf{r}} \tag{44}$$

and the transmitted waves are

$$\mathbf{E}_{2+}(\mathbf{r}) = \mathbf{u}_y E_{2+} e^{-j\mathbf{k}_{2+}\cdot\mathbf{r}} \tag{45}$$

$$\mathbf{H}_{2+}(\mathbf{r}) = (\mathbf{u}_z \sin\theta_2 - \mathbf{u}_x \cos\theta_2)\frac{E_{1+}}{\eta_1} e^{-j\mathbf{k}_{2+}\cdot\mathbf{r}} \tag{46}$$

For TM polarization the incoming waves are

$$\mathbf{H}_{1+}(\mathbf{r}) = \mathbf{u}_y \frac{E_{1+}}{\eta_1} e^{-j\mathbf{k}_{1+}\cdot\mathbf{r}} \tag{47}$$

$$\mathbf{E}_{1+}(\mathbf{r}) = (-\mathbf{u}_z \sin\theta_1 + \mathbf{u}_x \cos\theta_1)\frac{E_{1+}}{\eta_1} e^{-j\mathbf{k}_{1+}\cdot\mathbf{r}} \tag{48}$$

and the reflected waves are

$$\mathbf{H}_{1+}(\mathbf{r}) = -\mathbf{u}_y \frac{E_{1-}}{\eta_1} e^{-j\mathbf{k}_{1+}\cdot\mathbf{r}} \tag{49}$$

$$\mathbf{E}_{1+}(\mathbf{r}) = (\mathbf{u}_z \sin\theta_1 + \mathbf{u}_x \cos\theta_1) E_{1-} e^{-j\mathbf{k}_{1+}\cdot\mathbf{r}} \tag{50}$$

and the transmitted waves are

$$\mathbf{H}_{2+}(\mathbf{r}) = \mathbf{u}_y \frac{E_{2+}}{\eta_2} e^{-j\mathbf{k}_{1+}\cdot\mathbf{r}} \tag{51}$$

$$\mathbf{E}_{2+}(\mathbf{r}) = (-\mathbf{u}_z \sin\theta_1 + \mathbf{u}_x \cos\theta_1) E_{2+} e^{-j\mathbf{k}_{1+}\cdot\mathbf{r}} \tag{52}$$

These equations can be simplified by calculating the transverse impedance and the wave vector by comparing off-axis TE- and TM-mode equations with on-axis equations

$$\eta_{ti} = \frac{\eta_i}{\cos\theta_i}, \qquad \text{TE} \tag{53}$$

$$\eta_{ti} = \eta_i \cos\theta_i, \qquad \text{TM} \tag{54}$$

$$k_i = \eta_i \sqrt{\epsilon_1} \cos\theta_i \tag{55}$$

and the reflection coefficient is

$$R = \frac{\eta_{t2} - \eta_{t1}}{\eta_{t2} + \eta_{t1}} \tag{56}$$

2.3.4 Omnidirectional bandgaps

The symmetries of one-dimensional periodic structures do not allow perfect bandgaps in a general case for off-axis propagation. Still it is possible to have omnidirectional bandgap in a multilayer film when some additional requirements are fulfilled. The first requirement is that the dielectric constants of both materials in multilayer film have to be higher than on the medium where the multilayer film is. The second requirement is that the contrast between the dielectric constants of both materials have to be large enough.

2.4 Two-dimensional bandgap structures

The field patterns inside a bandgap structure have to be inspected to explain why TE and TM modes have different dispersion relations and how different lattices affect the modes. Concentration factor [6] tells how large part of the energy of the (electric) field in that band is in the parts of the bandgap structure which has higher relative permittivity

$$\text{concentration factor} = \frac{\int_{\epsilon_2} d^3\mathbf{r}\epsilon(\mathbf{r})|\mathbf{E}(\mathbf{r})|^2}{\int d^3\mathbf{r}\epsilon(\mathbf{r})|\mathbf{E}(\mathbf{r})|^2} \tag{57}$$

The higher the difference is in the concentration factor between neighbouring bands, the larger the bandgap between them is. This means that structures where the energy doesn't concentrate on that mode doesn't have large bandgaps for that mode. Later we see that to get large bandgap for TE and TM modes in the same frequency range we need to make a compromise structure to let both modes energy field concentrate.

3 Numerical modeling of finite one-dimensional bandgap structures

3.1 Introduction

For studying properties of periodic structures, both infinite and finite cases are studied. The reflection and transmission of a finite multilayer film is solved by calculating the overall impedance of the bandgap structure. Figure 6 shows an example of a one-dimensional bandgap structure.

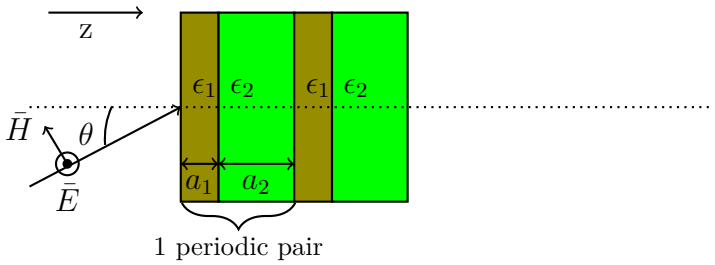

Figure 6: Multilayer film with n periodic pairs. A periodic part consist of two sequential layers with permittivities ϵ_1 and ϵ_2 and thicknesses a_1 and a_2

Equation (28) describes the equation for total electric field in a film. Based on that, the equation for the total electric field in the other boundary of the film is

$$E_1 = a_1 e^{jk_{z1}(z+a_1)} + b_1 e^{-jk_{z1}(z+a_1)} \tag{58}$$

Based on equation (32), the magnetic field in the same location is

$$H_1 = -\frac{k_{z1}}{\omega\mu} a_1 e^{jk_{z1}(z+a_1)} + \frac{k_{z1}}{\omega\mu} b_1 e^{-jk_{z1}(z+a_1)} \tag{59}$$

Equations for the field amplitudes E_{1+} and E_{1-} at point $z = 0$ can be solved using previous two equations

$$E_{1+} = \frac{1}{2}\left(E - \frac{\omega\mu}{k_{z1}} H\right) \tag{60}$$

$$E_{1-} = \frac{1}{2}\left(E + \frac{\omega\mu}{k_{z1}} H\right) \tag{61}$$

So the equation for the total electric field in the next boundary is given by

$$E(z+a_1) = \frac{1}{2}\left(E(z) - \frac{\omega\mu}{k_{z1}} H(z)\right) e^{ika_1} + \frac{1}{2}\left(E(z) + \frac{\omega\mu}{k_{z1}} H(z)\right) e^{-ika_1} \tag{62}$$

Similar equation can be derived for total magnetic field. Finally this can be transformed into a matrix form

$$\begin{pmatrix} E_1 \\ H_1 \end{pmatrix} = \mathbf{M_1} \begin{pmatrix} E_2 \\ H_2 \end{pmatrix} = \begin{pmatrix} \cos k_1 a_1 & i\eta_1 \sin k_1 a_1 \\ i\frac{1}{\eta_1} \sin k_1 a_1 & \cos k_1 a_1 \end{pmatrix} \begin{pmatrix} E_2 \\ H_2 \end{pmatrix}, \tag{63}$$

Similar of equation can be obtained also in the next layer

$$\begin{pmatrix} E_2 \\ H_2 \end{pmatrix} = \mathbf{M_{II}} \begin{pmatrix} E_3 \\ H_3 \end{pmatrix} \tag{64}$$

and the relationship between the fields on the first and third medium reads

$$\begin{pmatrix} E_1 \\ H_1 \end{pmatrix} = \mathbf{M_I} \begin{pmatrix} E_2 \\ H_2 \end{pmatrix} = \mathbf{M_I M_2} \begin{pmatrix} E_3 \\ H_3 \end{pmatrix} \tag{65}$$

This kind of approach is called Transfer Matrix Method (TMM). We can simplify calculations by turning the matrix equation to recursive equation for structure impedance. Using these equations to solve the impedance for one layer using relationship $\eta_i = \frac{E_i}{H_i}$ forms a recursive equation

$$Z_i = \eta_i \frac{Z_{i+1} + j\eta_i \tan k_i a_i}{\eta_i + jZ_{i+1} \tan k_i a_i} \tag{66}$$

Total impedance is calculated by starting from the end of the periodic structure, calculating the impedance of the current layer and substituting the impedance to the next layer equation until the first medium is reached. Reflection coefficient is the ratio of the amplitudes of incoming and reflected waves. Finally, [8] the reflection coefficient for the whole structure is obtained as

$$R_k = \frac{\eta_k - \eta_1}{\eta_k + \eta_1} \tag{67}$$

Here $k, k = 1, 2, 3, ...$ is the k:s layer in the n layer structure.

3.2 Bandgap size change with different dielectric constants and layer widths

The size of the bandgaps of one-dimensional bandgap structure depends on two factors: the fill factor of the material and the contrast between the two layer materials and contrast between layer materials and the medium where the bandgap structure is. The fill factor is the ratio of the material with higher dielectric constant against the width of one periodic pair

$$\text{Fill factor} = \frac{a_1}{a_1 + a_2} \tag{68}$$

Because the location of the stopbands and their size is proportional to the width the of periodic pair, we use the gap-midgap ratio to categorise stopbands. This is the ratio of the width of the bandgap to the middle frequency of the bandgap

$$\text{Gap-midgap ratio} = \frac{\Delta\omega}{\omega_m} \tag{69}$$

3.3 Dispersion relation with different material parameters

3.3.1 Bandgap size

As this work mostly focuses on the reflection of bandgap structures, we are very interested on what kind of fill factor gives the biggest bandgap. Figure 7 contains sizes of the first bandgap with different dielectric constant values for the material with higher dielectric constant and different fill factors. The maximal bandgap size is marked with a solid black line.

The black line in the figures corresponds closely to the quarter-wave stack structure. The midgap frequency of a quarter-wave stack is

$$\omega_m = \frac{n_1 + n_2}{4n_1n_2} \cdot \frac{2\pi c}{a} \tag{70}$$

and the gap-midgap ratio is

$$\frac{\Delta\omega}{\omega_m} = \frac{4}{\pi} \sin^{-1}\left(\frac{|n_1 - n_2|}{n_1 + n_2}\right) \tag{71}$$

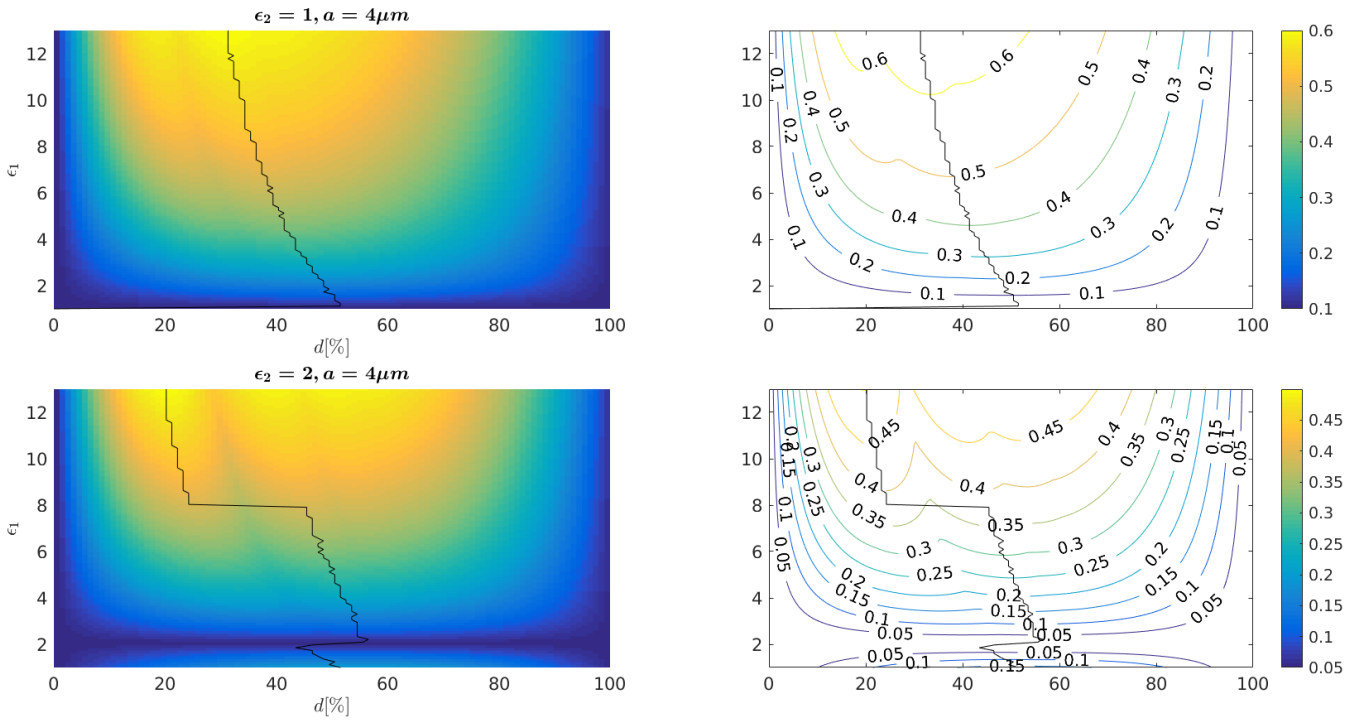

Figure 7: Bandgap size of the structures with different fill factors. On the top with no constranst between the lower dielectric constant and air and on the bottom with a contrast of two

3.3.2 Effect of the number of layers

In practice there are no infinitely periodic structures. In many cases thin structures are preferred to save material costs and to use bandgap structures in applications that demand small dimensions. Figure 8 represents the dispersion relation of an infinite bandgap structure with 2 to 1 ratio refractive indices and the fill factor of 1/3.

Next the size of the first stopband of this structure is compared with the size of the stopbands when the structure has finite number of layers.

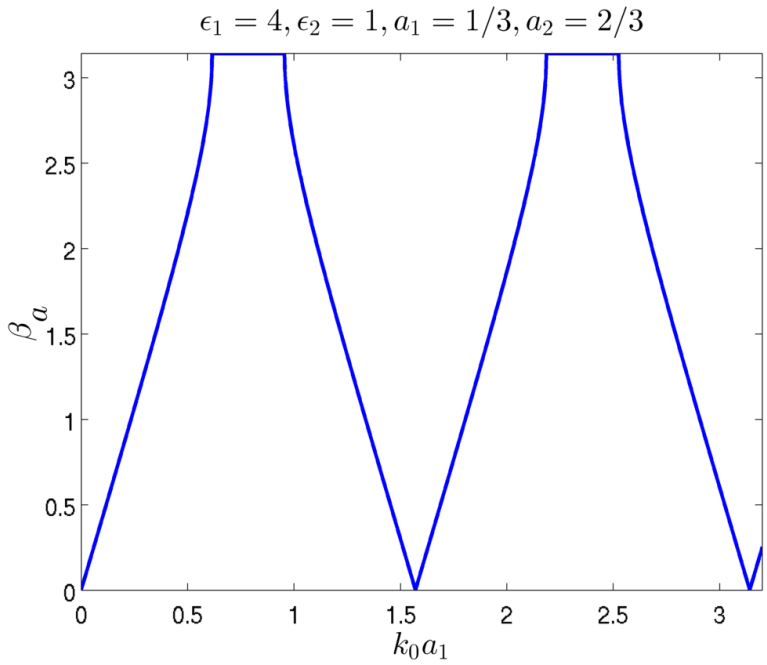

Figure 8: Dispersion relation for an infinite one-dimensional bandgap structure where β is the Floquet vector

3.3.3 Adding a defect layer to bandgap structure

During manufacturing of periodic structures there is always a chance that some defect is introduced into the system. In this example, the layer in the middle of a periodic structure is twice of its original width. The system is in Figure 9 and the reflection coefficients for perfect and imperfect bandgap structures are shown in Figure 10.

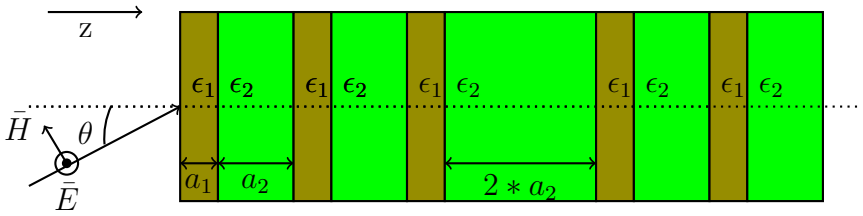

Figure 9: Periodic structure with one defect layer

Comparing Figure 10 to Figure 8, we can see that the bandgaps with 11 pairs are about the same size and are in the same locations than in the infinite case. The defect layer does not seem to decrease the size of the bandgap, but brings passband frequency in the middle of the bandgap.

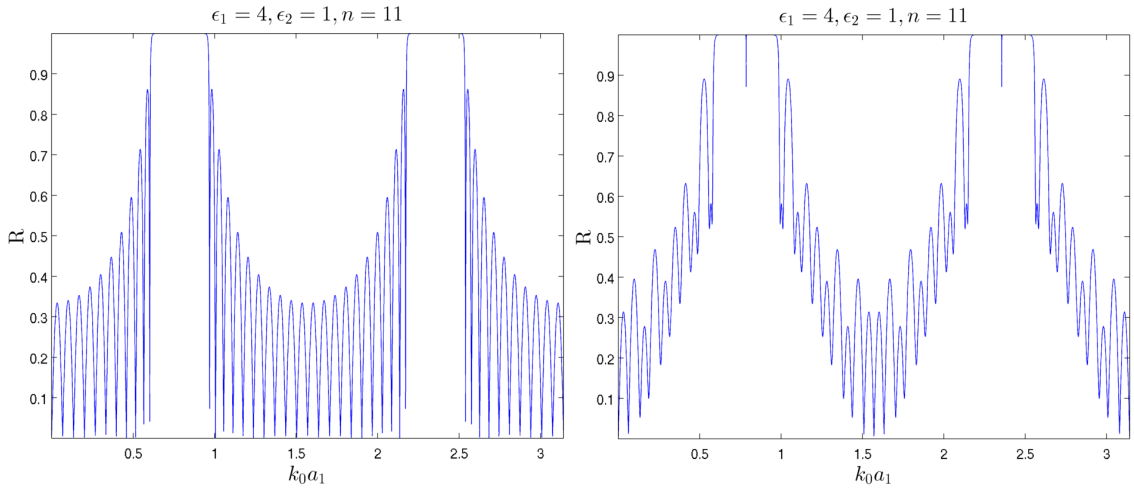

Figure 10: Difference in the reflection coefficient when a defect layer is introduced. Here n is the number of layer pairs

3.3.4 Layers with imperfect widths

In real world scenarios the widths are never perfect because of limited accuracy. The effect of manufacturing imperfections are modelled by adding Gaussian noise to the widths of each of the layers of multilayer structure. The mean is kept at zero and the variance is varied.

Looking through Figure 11, even moderately large noise levels don't break the bandgap of the bandgap structure.

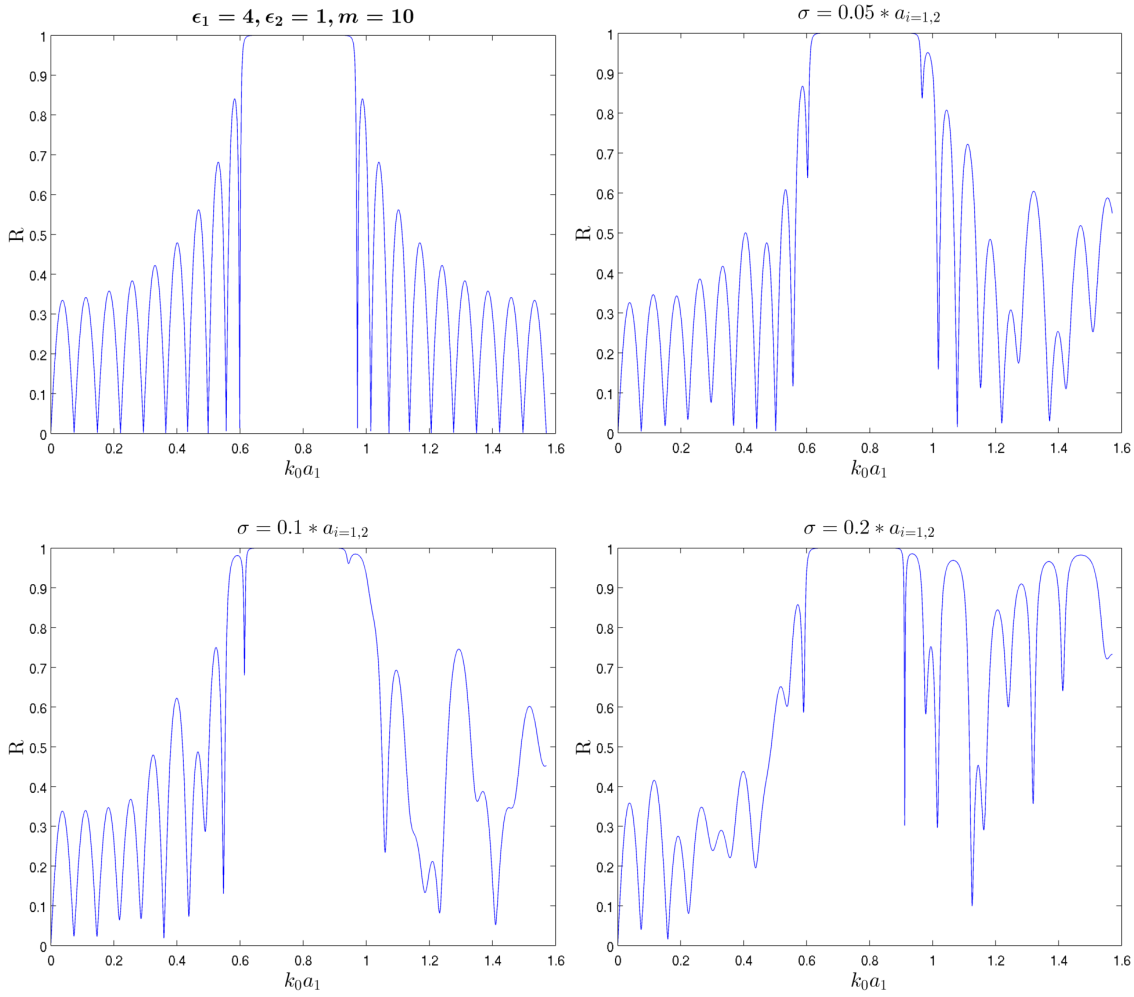

Figure 11: Reflectivity in the first bandgap area without noise(upper left) and withfew different noise variance levels

3.3.5 Effect of the incidence angle

In real world scenarios the electromagnetic wave usually doesn't propagate parallel to the normal of the boundary. The wave angle changes the bandgap size and place as the bandgap structure loses some of its periodicity. With zero angle the TE and TM modes have the same behavior, but when the angle increases, the cases separate. Effect of the incoming wave angle to the boundary normal was first tested with a one-dimensional bandgap structure with TE and TM waves that are coming in 0, 20 and 40 degrees angle. The reflective of the first bandgap are shown in Figure 12.

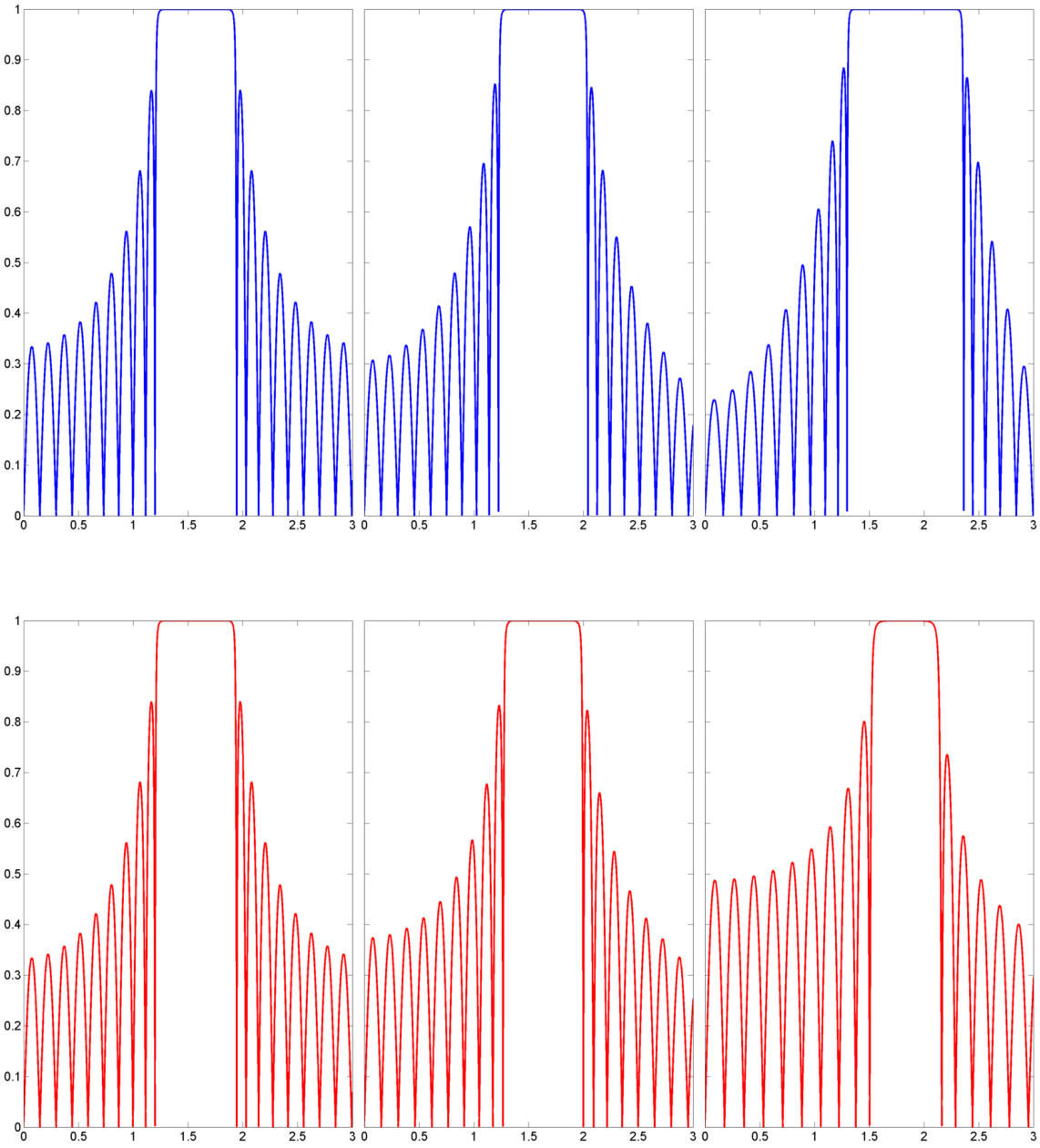

Figure 12: Bandgap size for TE (top) and TM (bottom) modes with different angles. From left to right: angle is 0, 20 and 40 degrees

Looking at the figures, the effect is clearly different between the TE and TM modes. On both modes the stopband is slowly moving to higher frequencies as the angle is increased. With the TE wave, the stopband also increases in size. For the TM wave, on the other hand, the bandgap size is decreasing as the angle is increased.

The goal would be to find a one-dimensional structure with a bandgap that doesn't depend on the incoming wave angle or its mode. As previously mentioned this kind of bandgap is called omnidirectional bandgap. Figures 13 and 14 show the first bandgap of two different one-dimensional bandgap structures with different angles.

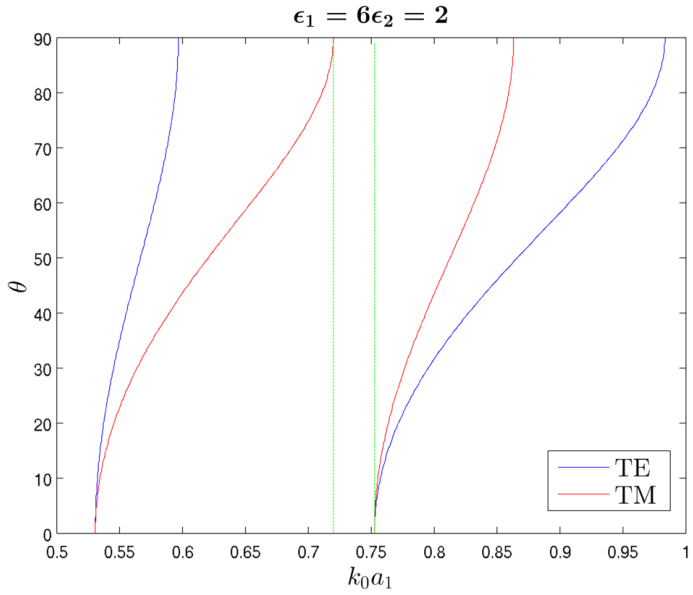

Figure 13: Bandgap size for the TE and TM modes with different incoming angles in a very large (n = 100) bandgap structure

To get an omnidirectional bandgap, both of the materials in the bandgap structure have to have different dielectric constants than the medium where the bandgap structure is. Also the constranst between the materials and between the materials and the medium background have to be large enough.

The incoming angle also has an effect on the difference between infinite and finite models of a bandgap structure. Figure 15 shows the difference between a very large($n > 100$) structure and a smaller structure in normal and logarithmic scales when comparing the size off the first bandgap. The value 100% means that the structure doesn't have 100% reflectivity at all in the frequencies of the first bandgap.

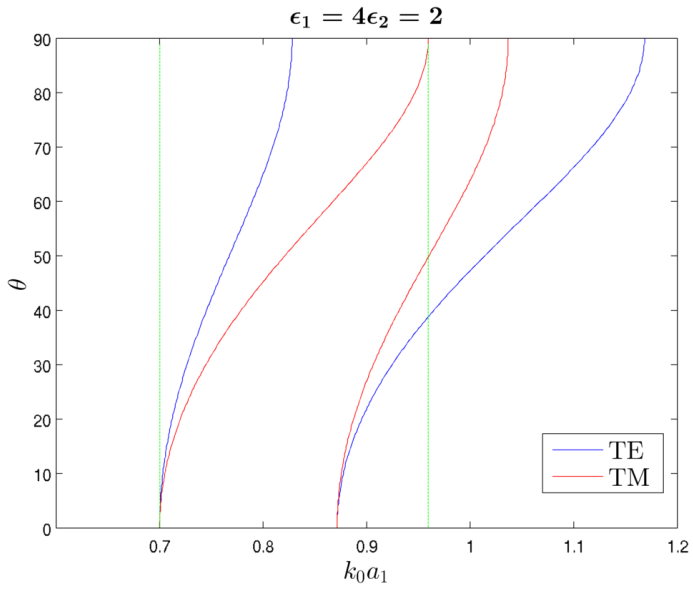

Figure 14: Bandgap size for the TE and TM modes with different angles in a very large (n = 100) bandgap structure

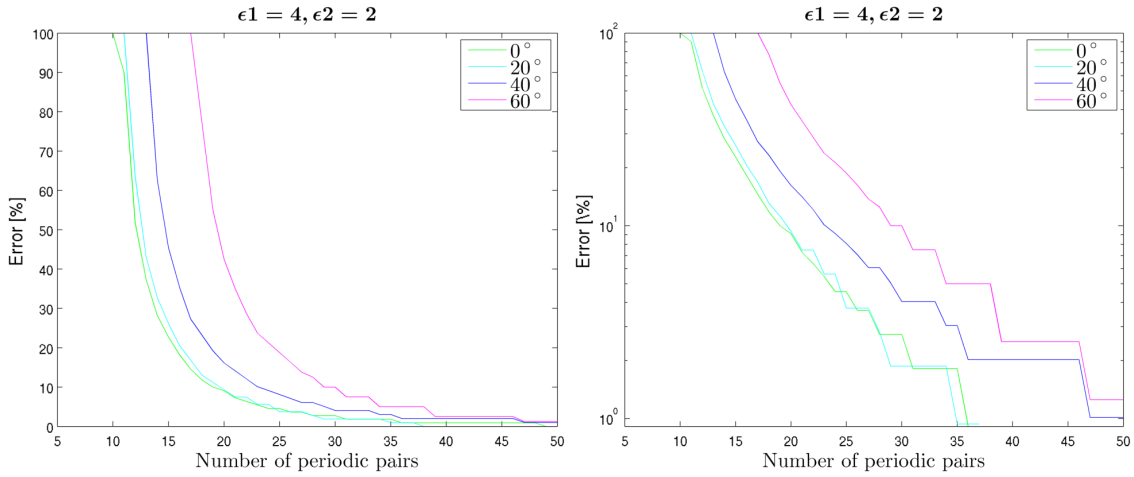

Figure 15: Effect of an incident angle to bandgap size in a finite bandgap structure

4 Numerical modeling of two-dimensional bandgap structures

Two-dimensional bandgap structures introduce a lot more complications to calculations compared to one-dimensional case. The almost infinite number of different geometries compared to a layer on the top of the layer structure makes general analytical approach impossible and brings a lot of challenges to numerical modeling. Indeed, there are many different numerical techniques for modeling bandgap structures. One of the most widely used method is the plane wave method [9]. It focuses on solving Helmholtz equation by treating the electric or magnetic field as an infinite sum of plane waves using Fourier composition. One other popular method is the Finite-Difference Time-Domain Method(FDTD)[10].

The numerical modeling method that was chosen to be used in this work was Finite Element Method.

4.1 Finite Element Method

4.1.1 Introduction

FEM is a numerical technique for solving boundary value problems of partial differential equations in arbitrary simulation area. FEM widely can be used easily in many different physical problems, for example, in heat transfer problems or beam stress problems.

4.1.2 Equation

Combining Maxwell's equations (8) and (9), and eliminating the magnetic field, we get the vector Helmholtz equation for the electric field

$$\nabla \times \frac{1}{\mu_r} \nabla \times \mathbf{E} - k_0^2 \epsilon_r \mathbf{E} = 0, \quad \text{in } \Omega \tag{72}$$

where $k_0^2 = \omega^2 \mu_0 \epsilon_0$ is the free-space wave number and Ω is the domain of interest. As was discussed before an electromagnetic wave can be separated to two linear polarization case. For example in the TE case the electric and magnetic fields are of the form

$$\mathbf{E} = \hat{z} E_z \quad \text{and} \quad \mathbf{H} = -\frac{1}{j\omega\mu} \nabla \times \mathbf{E} \tag{73}$$

Inserting (73) to equation (72) gives a scalar equation for E_z

$$\nabla \cdot \frac{1}{\mu_r} \nabla E_z - k_0^2 \epsilon_r E_z = 0 \tag{74}$$

Similar equation can be written also for the magnetic field in the TM case. The general form of the equations is [11]

$$\nabla \cdot \frac{1}{p} \nabla U - k_0^2 q U = 0 \tag{75}$$

where

$$U(x,y) = E_z(x,y), \quad p(x,y) = \mu_r(x,y), \quad q(x,y) = \epsilon_r(x,y), \text{for TE} \tag{76}$$

and

$$U(x,y) = H_z(x,y), \quad p(x,y) = \epsilon_r(x,y), \quad q(x,y) = \mu_r(x,y), \text{for TM} \tag{77}$$

respectively.

4.1.3 Forming weak form

The Helmholtz equation (75), formed in the previous section, can be written in operator form

$$Lu - f = R = 0 \tag{78}$$

where L is a linear operator operating the unknown quantity u, f is a known excitation function and R is the residual. There are no real analytical ways of solving this equation for arbitrary geometries and materials. Instead of solving the equation analytically, we solve the equation with FEM and form a weak form of it. In the weak form the equation is not forced to be exact in every point, instead the weighted average of the residual is forced to be zero

$$\int_\Omega W(x) R(x) dx = 0, \tag{79}$$

where W is a testing or weighting function. By multiplying (74) with a testing function ϕ and integrating by parts, we obtain a weak form for the TE case

$$\int_\Omega \nabla \phi \cdot \frac{1}{\mu_r} \nabla E_z ds - \omega^2 \mu_0 \epsilon_0 \int_\Omega \phi \epsilon_r E_z = 0 \tag{80}$$

4.1.4 Meshing

The next step in the FEM solution is meshing. The simulation area is divided to smaller geometrical pieces. Electromagnetic field needs to be assumed to change slowly in small distances. The most widely used geometrical form in meshing is a triangle. Triangles are simple geometrical forms that don't have constrains for what kind of geometry they can be used to mesh. There are other options, for example, quadrilaterals that has their own advantages in specific situations.

As the basis function depend on the underlining mesh, how the structure is meshed and how many triangles are used have large effect on the accuracy of the solutions. They are a lot of different methods and programs to how to divide an area to triangles. As a rule of thumb at least five elements per wavelength are needed to obtain reasonable solutions, if piecewise linear basis functions are used. Most of the work in this work is done using Gmsh program.

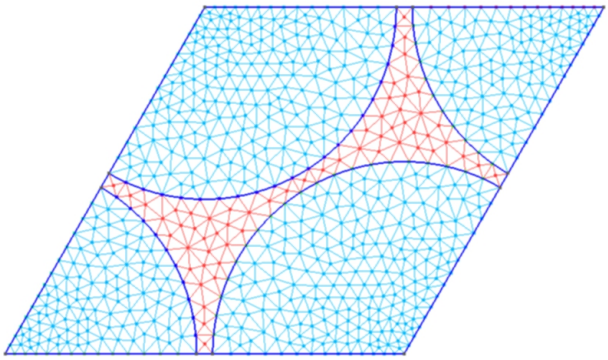

Figure 16: A two-dimensional mesh used to solve dispersion relations for a triangle lattice of air columns in dielectric material

4.1.5 Choosing basis functions

To find a numerical approximation for a function in a simulation area we need interpolation functions. These are called basis functions. Basis functions are used as substitutes for the real function so that

$$\tilde{u} \approx \sum_{j=1}^{N} u_j w_j \tag{81}$$

where u_j are the function coefficients and w_j are the basis functions. Most simple functions are node-based basis functions. In a two-dimensional case basis functions associated with triangular elements are used. These are linear functions that are

associated with one node of the mesh where their value is one and in all other nodes the value is zero.

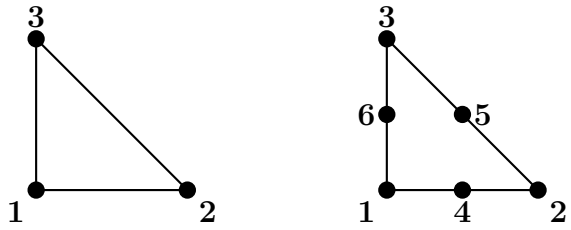

Figure 17: Node placements in reference element when using basis functions of the order of one (left) or two (right)

For choosing weighting functions the Galerkin method is used where the testing function and the basis functions are the same.

4.1.6 Solving eigenvalues

Finally when combining equations for each point in the mesh we get system matrix. To analyse this matrix and thus analyse the lattice that it represents, eigenvalues of the matrix are usually calculated. Eigenvalue λ of matrix $\mathbf{A}$ is value that has associated eigenvector $\mathbf{x}$ so that they fulfil equation

$$\mathbf{A}\mathbf{x} = \lambda\mathbf{x} \tag{82}$$

All the FEM calculations were done with using Matlab as scripting platform. For solving eigenvalues of the system matrix Matlab functions eig and eigs where used. Eigs is an iterative solver that starts from a randomised guess. It also wants to matrix used as input argument to be sparse which it is usually in FEM calculations. The results of the function is limited in that it gives the highest eigenvalues of the matrix. For more throughout look of eigenvalues eig can be used. In tests running this works FEM code with eigs and eig, eigs is much faster than the eig function and the accuracy is comparable.

4.2 Finite Element Method in periodic media

When dealing with periodic media, we had to add a periodic boundary condition to our equations. This boundary condition is based on the Bloch condition

$$U(r + R) = e^{ika}U(r) \tag{83}$$

Boundary nodes of the mesh of the lattice are separated to the left and right side. Idea is to get a matrix that has only one side of the boundary nodes and the other

side will be calculated from the Floquet-Bloch condition. Following the procedure in [12], this will be done by using an auxiliary matrix to transform the eigenvalue equation

$$\mathbf{P}^*\mathbf{S}\mathbf{P}\begin{pmatrix}\mathbf{u}\\ \mathbf{u}_l\\ \mathbf{u}_{lf}\\ \mathbf{u}_f\end{pmatrix} = k_0^2\mathbf{P}^*\mathbf{T}\mathbf{P}\begin{pmatrix}\mathbf{u}\\ \mathbf{u}_l\\ \mathbf{u}_{lf}\\ \mathbf{u}_f\end{pmatrix} \tag{84}$$

For example, with a square lattice shown in Figure 18, we obtain

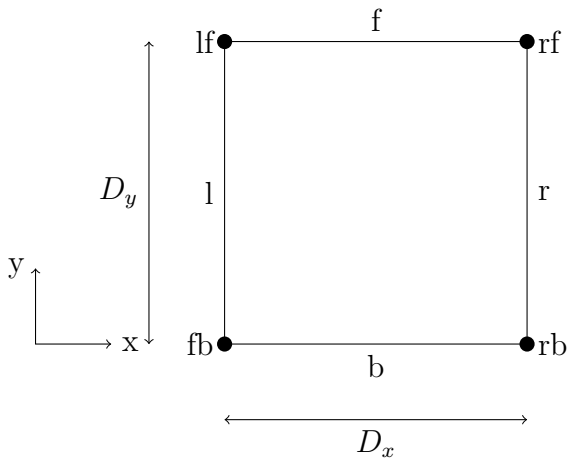

Figure 18: Square lattice unit cell

$$\begin{pmatrix}\boldsymbol{u}\\ \mathbf{u}_l\\ \mathbf{u}_{lf}\\ \mathbf{u}_{lb}\\ \mathbf{u}_f\end{pmatrix} = \mathbf{P_1}\begin{pmatrix}\boldsymbol{u}\\ \mathbf{u}_l\\ \mathbf{u}_{lf}\\ \mathbf{u}_f\end{pmatrix} = \begin{pmatrix}\mathbf{1} & \mathbf{0} & \mathbf{0} & \mathbf{0}\\ \mathbf{0} & \mathbf{1} & \mathbf{0} & \mathbf{0}\\ \mathbf{0} & \mathbf{0} & \mathbf{1} & \mathbf{0}\\ \mathbf{0} & \mathbf{0} & \mathbf{1}\exp(-i\beta_y D_y) & \mathbf{0}\\ \mathbf{0} & \mathbf{0} & \mathbf{0} & \mathbf{1}\end{pmatrix}\begin{pmatrix}\boldsymbol{u}\\ \mathbf{u}_l\\ \mathbf{u}_{lf}\\ \mathbf{u}_f\end{pmatrix}, \tag{85}$$

where $\mathbf{u}$ is the field solution, indices l, r, b, f are for left, right, bottom and upper edges, and $\mathbf{1}$ ja $\mathbf{0}$ are the unit and zero matrices with suitable dimensions.

4.3 Dispersion relations of different lattices

In an one-dimensional bandgap structure the structure was changed by using different layer widths and using materials with different dielectric constants. In the two-dimensional case the geometry of a periodic unit cell has to be taken account. Theoretically there is almost infinitely many geometries to choose form. In practice the manufacturing techniques limit greatly what kind of geometries can be used. Some of the most popular and widely studied geometries are shown in Figure 19.

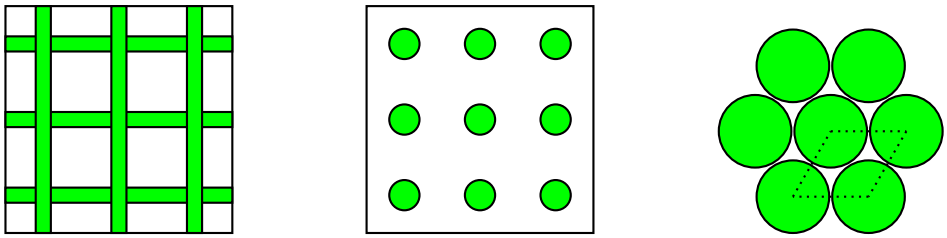

(a) Square array of veins (b) Square array of columns (c) Triangular lattice of columns

Figure 19: Some common two-dimensional bandgap structures

In the two-dimensional case the angle of the electromagnetic wave have to be always taken into account. This means that again the TE and TM modes have to be studied separately. The modes behave differently on different geometries and for example, a mode can have a bandgap in a geometry where the other mode doesn't have a bandgap. Figure 20 shows the dispersion relation for a bandgap structure with a square array of dielectric pillars in air. As the figure shows, even with a relatively high dielectric constant there is no bandgap for either mode.

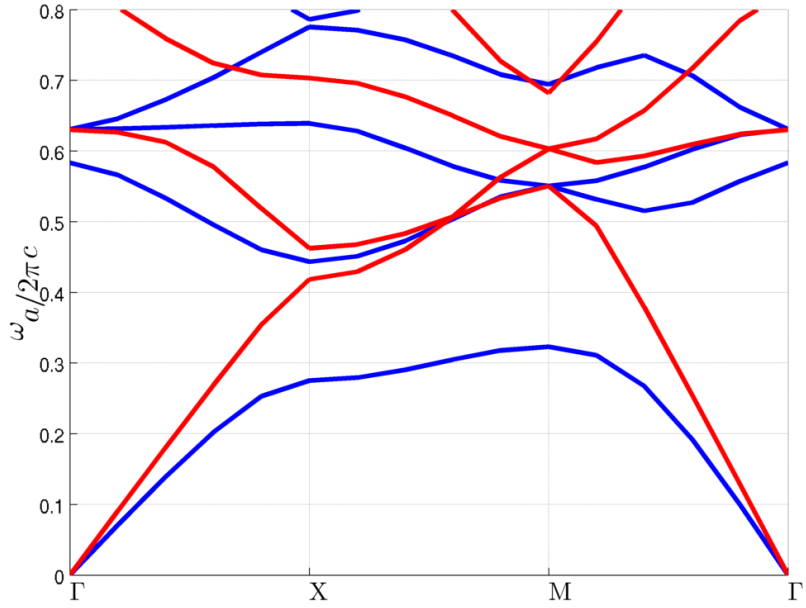

Figure 20: Dispersion relation for square array of columns with TE and TM mode waves

Figure 21 shows the dispersion relation for the bandgap structure with a triangle array of air pillars in a dielectric material which has bandgap for both electromagnetic modes.

Figure 22 shows the dispersion relation for the bandgap structure with dielectric veins in a square lattice in air. In this case the TM mode has a bandgap, but there is no bandgap for the TE mode

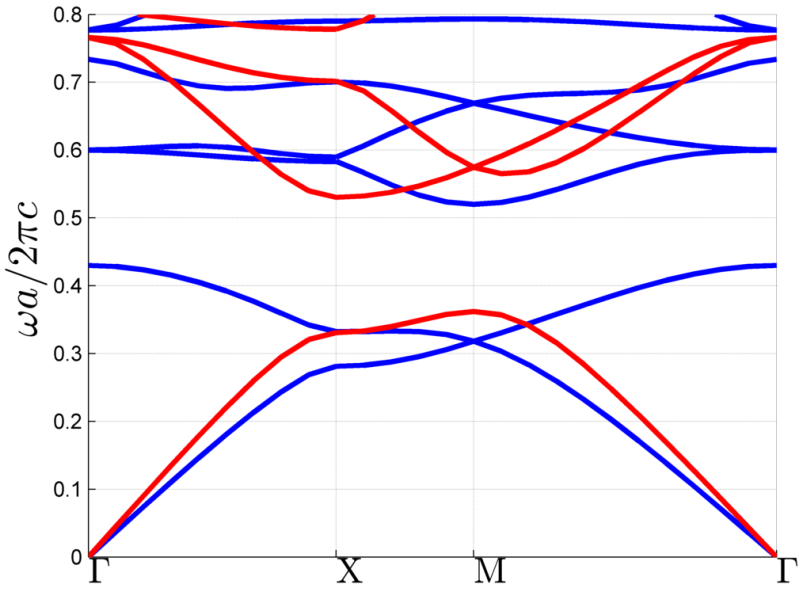

Figure 21: Dispersion relation for a triangle array of columns with TE and TM mode waves

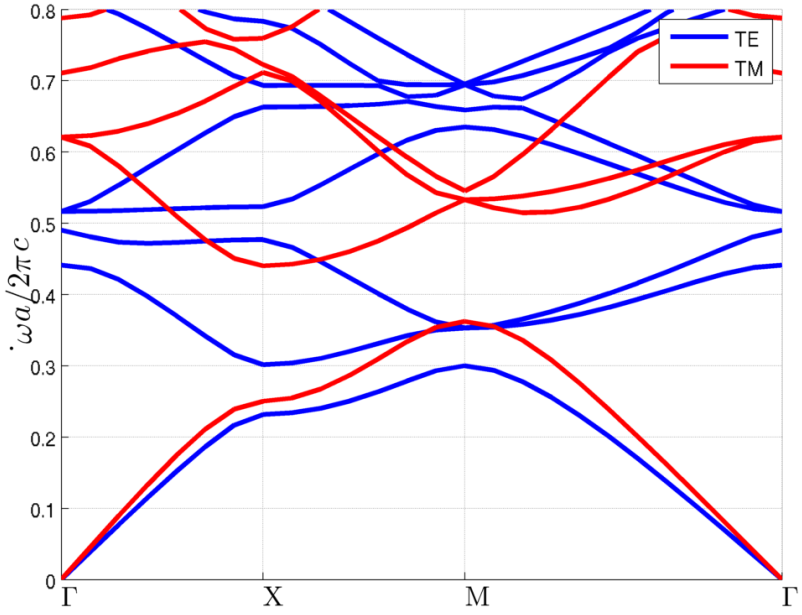

Figure 22: Dispersion relation for a square array of dielectric veins in air with TE and TM mode waves

The fill factor can be still used as an analysing tool. In the two-dimensional case it means the ratio of the areas of the material with higher dielectric constant compared to the area of the whole periodic unit cell.

To further examine why the bandgaps are forming differently for TE and TM mode waves we plot simulation of the electric and magnetic fields inside photonic crystal. For this simulation square array of columns are used. To see clearer how the amplitude

changes 3x3 unit structure is used. Magnetic field for single point in Brillouin zone in first and second band in photonic band structure are plotted in Figure 23 and electric field in the same point in first and second band in Figure 24. First and second band are also called dielectric and air band[6].

The color in the Figures 23 and 24 refer to the relative amplitude of the magnetic or electric field on that spot. Comparing the figures to each other we can see clear difference how fields are concentrating in the photonic crystal structure. To quantify this visual representation we can refer back to previously discussed equation (57) for concentration factor.

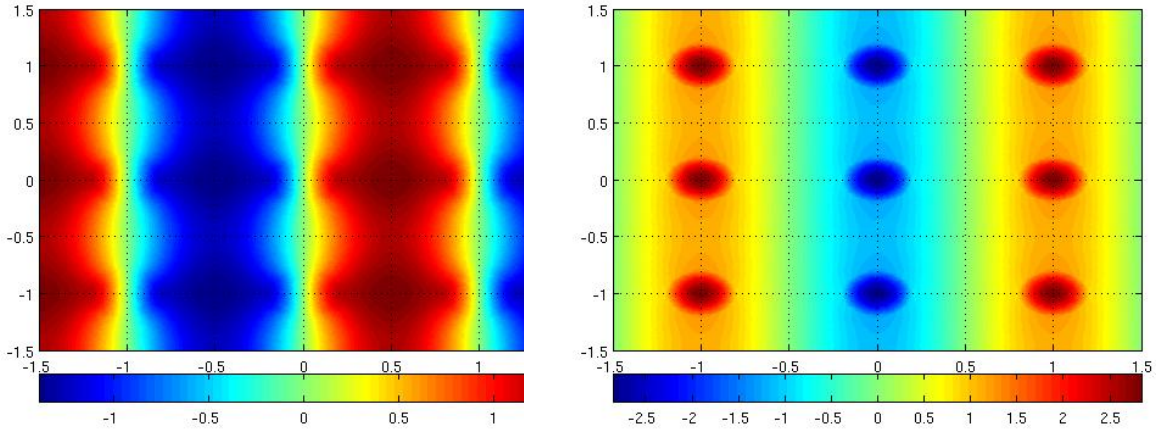

(a) 1. band (b) 2. band

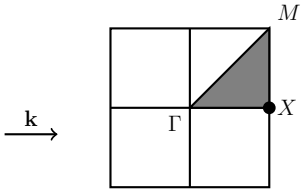

Figure 23: Magnetic fields in TM mode

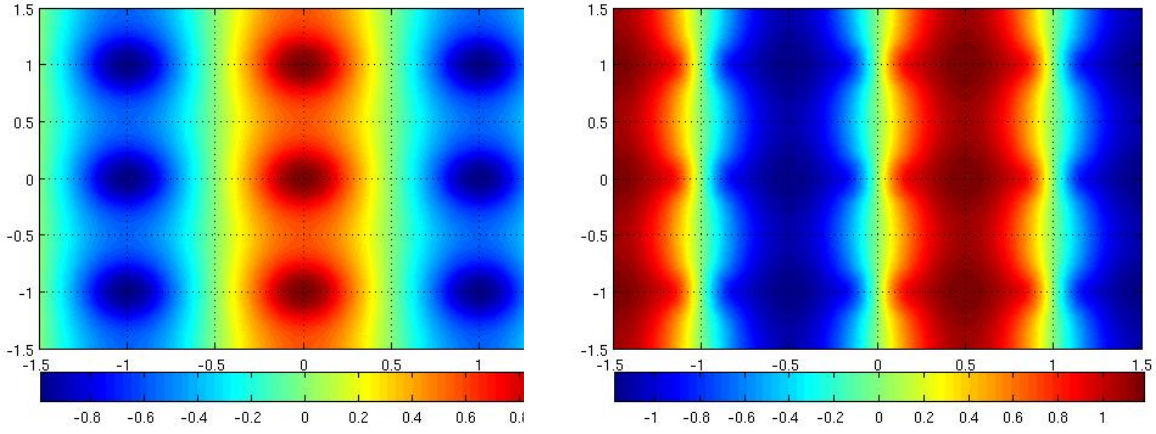

(a) 1. band (b) 2. band

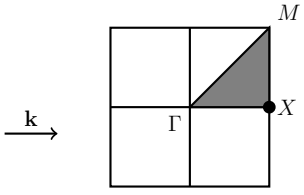

Figure 24: Electric fields in TE mode

5 Conclusions

In this work theoretical methods of analysing bandgap structures and their effect to electromagnetic fields passing through them where studied. Work focused in two major area: one-dimensional case where structures where multilayer films and two-dimensional case. Objective was to show how analytical and numerical methods help to find geometry and material parameters to get certain stopband.

In one-dimensional case reflectivity equations show that the reflectivity of the structure is same for TE and TM cases when the angle of the incidence in perpendicular. But as soon as the angle is different from that TE and TM cases start to diverge. In both cases the stopbands start to move to higher frequencies. For TE case the stopbands also started to widen and for TM case opposite was true as the stopband for it starts to shrink as the angle of incidence grew.

Analysing of two-dimension case was mainly done by using FEM. From simulation results we noticed that TE and TM cases had completely different reflectivity profile as we could presume from one-dimensional case. But unlike in the one-dimensional case, here with specific geometries and with high enough dielectric constant contrast TE and TM could have bandgaps at the same wavelengths for all angles which was called absolute band gap.

Future directions for this work would be compare the effectiveness of different numerical methods compared to Finite Element Method. Other interesting continuation for this work would be to research finding optimal geometries by using different machine learning and optimization algorithms like for example genetic algorithms [13].

References

[1] E. Yablonovitch, "Inhibited spontaneous emission in solid-state physics and electronics," *Phys. Rev. Lett.*, vol. 58, pp. 2059–2062, May 1987.

[2] E. Rephaeli, A. Raman, and S. Fan, "Ultrabroadband photonic structures to achieve high-performance daytime radiative cooling," *Nano Letters*, vol. 13, no. 4, pp. 1457–1461, 2013.

[3] "Early lights," *Nature materials, editorial*, vol. 11, no. 12, p. 995, 2012.

[4] A. Sihvola and I. Lindell, *Sähkömagneettinen kenttäteoria - 2.Dynaamiset kentät*. Otatieto, 2004.

[5] D. L. Sidebottom, *Fundamentals of condensed matter and crystalline physics*. New York: Cambridge University Press, 2012.

[6] J. D. Joannopoulus, R. D. Meade, and J. N. Winn, *Photonic Crystals*. Princeton University Press, 1995.

[7] L. Novotny, *Principles of nano-optics*. Cambridge University Press, 2006.

[8] E. Hecht, *Optics*. Addison Wesley Longman, Inc., 2002.

[9] D. W. Prather, *Photonic crystals : theory, applications, and fabrication*. New Jersey, N.J. : Wiley, 2009.

[10] A. Taflove and S. C. Hagness, *Computational electrodynamics: The finite-difference time-domain method*. Boston, MA: Artech House, 2005.

[11] J. L. Volakis, A. Chatterjee, and L. C. Kempel, *Finite Element Method for Electromagnetic - Antennas, Microwave Circuits and Scattering applications*. IEEE Press, 1998.

[12] A. Nicolet, S. Guenneau, C. Geuzaine, and F. Zolla, "Modelling of electromagnetic waves in periodic media with finite elements," *Journal of Computational and Applied Mathematics*, vol. 168, no. 1-2, pp. 321–329, 2004.

[13] G. A. Gazonas, D. S. Weile, R. Wildman, and A. Mohan, "Genetic algorithm optimization of phononic bandgap structures," *International Journal of Solids and Structures*, vol. 43, no. 18–19, pp. 5851 – 5866, 2006.